DALTON

X-Ray–neutron diffraction study of the electron-density distribution in *trans*-tetraaminedinitronickel(II) at 9 K: transition-metal bonding and topological analysis†

Bo B. Iversen,*[a] Finn K. Larsen,[a] Brian N. Figgis[b] and Philip A. Reynolds[c]

[a] *Department of Chemistry, Aarhus University, DK-8000 Aarhus C, Denmark*
[b] *Department of Chemistry, University of Western Australia, Nedlands, WA 6907, Australia*
[c] *Research School of Chemistry, Australian National University, Canberra, ACT 0200, Australia*

A quantitative description of transition-metal bonding has been obtained through combined analysis of 9(1) K X-ray and 13(1) K time-of-flight neutron diffraction data. It is shown that a simple valence-orbital model is too crude an approximation adequately to describe the electron-density distribution of $Ni(ND_3)_4(NO_2)_2$. To exhaust more fully the information present in the very-low-temperature diffraction data, a more flexible electron-density model was used. Quantitative measures describing the bonding in the complex have been achieved through topological analysis of the derived static model density. To study the effects of co-ordination and intermolecular interactions, comparisons were made with good-quality wavefunctions calculated for free nitrite and ammonium ions. Both ligands appear co-ordinated through predominantly electrostatic interactions. Contrary to previous studies of $Ni(ND_3)_4(NO_2)_2$, the topological analysis revealed that the metal–ligand interactions, besides cylindrical σ contributions, also have non-cylindrical π contributions to the covalent part of the bonding. Plots of the Laplacian of the electron density were used to locate regions of charge concentration and charge depletion in the valence regions of the atoms in the molecule. For all atoms, maxima in the valence-shell charge concentration are found in accord with the simple Lewis electron-pair concept of bonded and non-bonded charge concentrations. The study demonstrates that X-ray diffraction data measured carefully at very low temperatures have sufficient precision to allow for a reliable and detailed topological analysis of transition-metal electron-density distributions.

Quantitative descriptions of metal–ligand bonding in transition-metal complexes can be obtained through analysis of molecular electron-density distributions (EDDs).[1] These can be determined from experiment by accurate X-ray diffraction measurements preferably in combination with neutron diffraction measurements on the same compound (X–N method). Previously we have carried out a combined X-ray and neutron diffraction study of diammonium hexaaquacopper(II) disulfate,[2] $(ND_4)_2Cu(OD_2)_6(SO_4)_2$ (ammonium copper Tutton salt, **1**), similar to the present one on $Ni(ND_3)_4(NO_2)_2$ **2**. In that study considerable improvements were obtained by collecting data at 9 K relative to a study done with liquid-nitrogen cooling[3] (≈85 K). At 9 K usual systematic errors such as thermal diffuse scattering (TDS) and anharmonic motion are suppressed to a point where they are negligible.[4] For the low-temperature data for **1** extra radial flexibility, besides the κ parameter normally used in experimental charge-density studies,[5] was necessary in order to obtain a satisfactory model. The very flexible model used in that study resulted in the coincidence of both the positional and thermal parameters obtained separately from the X-ray and neutron diffraction data. At higher temperatures discrepancies between X-ray and neutron parameters are observed due to temperature-dependent differences in systematic errors between the two experiments, and such discrepancies have often compromised the accuracy of X–N studies.

In the present study of compound **2** we have carried out 9(1) K X-ray diffraction and 13(1) K time-of-flight neutron diffraction measurements. In a preceding paper[6] details about the data acquisition, data reduction and the refined structural parameters were described.‡ It was shown that for **2** excellent agreement between positional and thermal parameters for the two experiments can be obtained. The root mean square (r.m.s.) difference between the U values ($\langle\langle(\Delta U_{ij})^2\rangle^{\frac{1}{2}}$) was as low as 0.000 50 Å^2 and $\langle(\Delta U_{ij}/\sigma_{ij})^2\rangle^{\frac{1}{2}} = 1.92$. Owing to the very low temperatures of the experiments the absolute differences between the thermal parameters are much smaller than what is normally obtained in studies using nitrogen cooling. For complex systems the faster but more complex time-of-flight neutron diffraction technique can produce structural parameters of a quality comparable to experiments with monochromatic neutrons. The excellent correspondence between the parameters derived separately from the X-ray and neutron data demonstrates that systematic errors in the data are small and this gives confidence in the deconvolution of the thermal motion from the X-ray data.

Recently it has been shown that, for systems as large as transition-metal complexes, neither current theoretical methods nor empirical modelling techniques are able to produce EDDs that fully do justice to the quality of the experimental data which can be produced by careful diffraction measurements at very low temperatures (≈10 K).[7] For the theoretical results this may be due to inadequate treatment of both e^-–e^- correlation and intermolecular effects, such as charge transfer and polarisation. In the case of the empirical EDD models it is clear that, although very flexible, they are still too rigid to fit all subtle density features. Much knowledge can therefore be gained

† *Non-SI unit employed*: au ≈ 4.36×10^{-18} J.

‡ Time-of-flight neutron diffraction data: 13(1) K, 40 three-dimensional data histograms, 2436 reflections for least squares, wavelength range $0.7 < \lambda < 4.2$ Å, $(\sin\theta/\lambda)_{max} = 1.17$ Å^{-1}, $a = 10.580(2)$, $b = 6.720(1)$, $c = 5.863(1)$ Å, $\beta = 114.82(1)°$, space group $C2/m$, $Z = 2$, μ_a(true absorption at $\lambda = 1.8$ Å) = 0.549 cm^{-1}, μ_s(total scattering) = 1.202 cm^{-1}, 78.5% deuteriation (refined), box-shaped crystals of side length 2.5 mm. X-Ray diffraction data: 9(1) K, Ag-Kα radiation ($\lambda = 0.5603$ Å), 9231 reflections measured, 4016 unique for least squares, $R_I = 0.023$, $(\sin\theta/\lambda)_{max} = 1.40$ Å^{-1}, $a = 10.647(2)$ Å, $b = 6.799(1)$ Å, $c = 5.891(1)$ Å, $\beta = 114.82(1)°$, μ_l(Ag-Kα) = 13.11 cm^{-1}, crystal boundaries ±(001) 0.13, ±(20−1) 0.09, (1−1−1) 0.12, (−2−41) 0.14, (010) 0.32 mm.

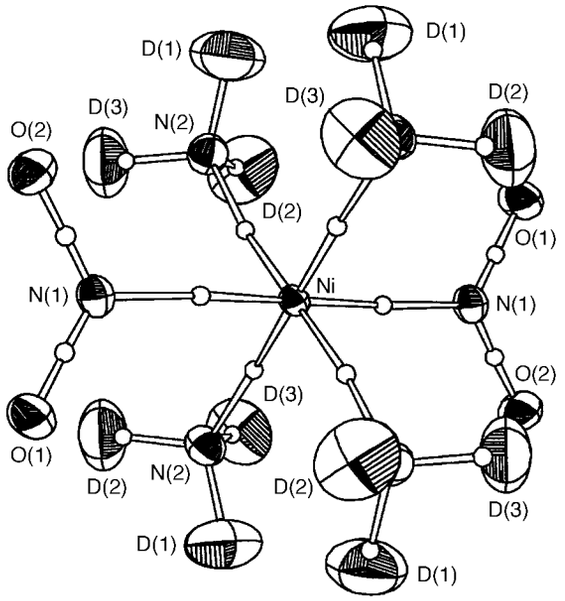

Fig. 1 An ORTEP[8] drawing of $Ni(ND_3)_4(NO_2)_2$ showing 90% ellipsoids and the atom-numbering scheme. Also shown are the bond critical points found in topological analysis of the static model density. Note the large zero-point thermal motion of the deuterium atoms relative to the heavier atoms

through detailed comparison of advanced empirical EDD models with results of high quality *ab-initio* calculations. We are presently carrying out extensive *ab-initio* calculations on **2** and in a forthcoming paper a full account of this aspect will be given.

The present compound was chosen further to probe the nature of the deficiencies in both theory and experimental models on a chemically more interesting system having ligands of quite different positions in the electrochemical series. It is found (Fig. 1) as a single molecular entity in the crystal and so it is expected that intermolecular effects on the molecular EDD are reduced and comparisons between theory and experiment can be enhanced relative to more ionic systems.

Furthermore compound **2** has been examined by a wealth of different methods including X-ray diffraction,[9] magnetochemical,[9b] spectroscopic,[9b] neutron diffraction,[10] polarised neutron diffraction experiments[11] and by *ab-initio* theoretical calculations.[12] This allows for a comparison with other experimental and theoretical results. The geometry and structural characteristics of the complex were discussed by Figgis *et al.*[9b] based on X-ray diffraction data collected at 130 K, and based on a limited set of neutron diffraction data collected at 4.2 K.[10] Overall the present study agrees well with the previous results. The most noteworthy difference is the more precise N–D bond lengths found in the present study. In the previous neutron diffraction study N–D 0.996(8), 1.045(12) and 1.005(11) Å compared to the present values of 1.015(1), 1.015(1) and 1.014(1) Å. The complex has a small but significant orthorhombic distortion [N(2)–Ni–N(2) 87.46(2)°]. Furthermore it has consistently been observed that the two N–O bonds are slightly different in length [N(1)–O(1) 1.244(1) and N(1)–O(2) 1.255(1) Å]. In the crystal structure there are hydrogen bonds between the ammonia deuterium atoms and the nitrite oxygen atoms. One oxygen atom [O(1)] has two hydrogen bonds [D(3) ··· O(1) 2.159(1) Å] and the other [O(2)] has four hydrogen bonds [D(1) ··· O(2) 2.175(1) and D(2) ··· O(2) 2.126(1) Å].

Figgis *et al.*[9c] further studied compound **2** by X-ray diffraction methods at 110 K, and found a valence-orbital model to be an adequate description of the improved data. The new 9 K data reveal that this is not really true. Comparison between the 110 and 9 K models directly shows the increased resolution gained by lowering the temperature of the experiment. At the same time we also now use X-ray diffraction in combination with neutron diffraction results. With the high quality of the low-temperature data and the inclusion of many high-order data, the valence-orbital model is now too inflexible. Chandler *et al.*[12] compared the 110 K experimental charge-density to *ab-initio* calculations and found broad agreement, although some notable differences were observed. The 110 K X-ray experiment yielded a very low nickel $3d_{xy}$ population and high 4p populations which were not reproduced by theory. It was speculated that this was due to mixing of a doubly excited state into the ground state through configuration interaction (CI), and to resolve this point a rigorous CI calculation seemed to be needed. The higher precision of the present data makes it possible partly to resolve this question. However, because it is necessary to introduce a very flexible electronic model properly to describe the data, it is no longer really meaningful to speak of pseudo-atom fragments and their associated orbital populations. We have instead attempted to use topological analysis on the static model total density derived from the X-ray data inspired by Bader's theory of atoms in molecules.[13] The theory of atoms in molecules has mostly been applied to fairly simple organic molecules which can be well described by theoretical methods. In recent years it has been shown that valuable topological information can also be obtained from experimentally derived EDDs of small organic molecules and simple metals.[14] However, because of the much greater complexity of transition-metal systems, little is known about the topological features of this important class of compounds. Numerous bonding models are in general use to describe the diversity found in transition-metal bonding. It would therefore be interesting to obtain a new view of transition-metal bonding through use of topological methods. This cannot be achieved from a study of a single complex, but if precise EDDs can be derived for a number of complexes, trends and characteristics of the topology of various bonding types may be found. In the present study we probe what kind of topological information can be reliably retrieved for transition-metal complexes from conventional diffraction data measured at very low temperatures (≈10 K).

Multipole Modelling

In this study we used the program XD.[15] It employs the Hansen and Coppens[16] multipole formalism in the description of the charge density. The atomic density contributions are parameterised into a core term, ρ_{core}, a spherical valence term, $\rho_{valence}$, and a set of multipolar functions as shown in equation (1). In the

$$\rho_{atom}(\mathbf{r}) = P_{core}\rho_{core} + P_{valence}\kappa^3\rho_{valence}(\kappa r) + \sum_{l=0}^{l_{max}} \kappa_l'^3 R_l(\kappa_l' r) \sum_{m=0}^{l} P_{lm\pm} d_{lm\pm}(\theta, \varphi) \quad (1)$$

standard model two κ expansion/contraction parameters are included for each atom: one modifies the radius of the spherical valence term and the second modifies the radius of the multipolar terms. The XD program also allows extra radial flexibility to be introduced in the modelling by use of separate κ parameters for each multipole order.

With the results of our study[2] of compound **1** in mind it was clear that we had to construct a very flexible electronic model properly to describe the present data. A number of models were refined but we only present detailed results for what we believe to be the best multipole model. This model contained full multipole expansions up to fourth order on Ni, up to third order on N(1), N(2), O(1) and O(2), and to second order on D(1), D(2) and D(3). On Ni a very flexible model containing two sets of multipoles was used. For N(1), the nitrite nitrogen atom, separate κ parameters were refined for all multipole orders. The other atoms only had two κ parameters refined. The two κ parameters were constrained to be the same on all three

Table 1 Electron-density parameters obtained from a refinement with the XD program: M refers to monopoles, D to dipoles, Q to quadrupoles, O to octapoles and H to hexadecapoles; for Ni two sets of multipoles (mul), with radial dependencies derived from 3d and 4s orbital products respectively, were used

Ni: $M1_{3d}$ 2.21(3), $Q0_{3d}$ −0.33(7), $Q2+_{3d}$ −0.03(4), $Q2-_{3d}$ −0.05(4), $H0_{3d}$ 0.116(6), $H2+_{3d}$ 0.151(5), $H2-_{3d}$ −0.179(5), $H4+_{3d}$ 0.012(4), $H4-_{3d}$ −0.124(4), $M1_{4s}$ 0.75(24), $Q0_{4s}$ 0.25(7), $Q2+_{4s}$ 0.02(4), $Q2-_{4s}$ 0.06(4), $H0_{4s}$ 0.127(6), $H2+_{4s}$ −0.09(5), $H2-_{4s}$ 0.17(5), $H4+_{4s}$ −0.04(4), $H4-_{4s}$ 0.122(4), κ_{3d} 1.09(1), κ_{4s} 1.00
O(1): M1 3.10(4), D1+ −0.046(7), D1− 0.002(7), Q0 −0.054(9), Q2+ −0.062(8), Q2− −0.020(7), O1+ 0.008(7), O1− −0.009(8), O3+ 0.004(6), O3− 0.002(6), κ(M1) 1.028(7), κ(mul) 1.38(12)
O(2): M1 3.14(4), D1+ −0.043(8), D1− −0.019(8), Q0 −0.041(10), Q2+ −0.034(8), Q2− −0.000(7), O1+ −0.004(8), O1− −0.006(8), O3+ 0.011(6), O3− 0.001(6), κ(M1) 1.109(7), κ(mul) 1.27(13)
N(1): M1 2.43(5), D1+ 0.056(9), D1− −0.011(7), Q0 −0.11(2), Q2+ 0.01(1), Q2− 0.01(1), O1+ 0.06(2), O1− 0.01(2), O3+ 0.17(3), O3− 0.01(2), κ(M1) 1.05(1), κ(D) 1.36(15), κQ 0.98(10), κ(O) 0.75(5)
N(2): M1 4.13(18), D0 0.21(5), D1+ 0.04(4), D1− 0.06(4), Q0, 0.11(3), Q1+ −0.03(3), Q1− 0.06(3), Q2+ −0.07(3), Q2− 0.00(3), O0, 0.17(4), O1+ 0.05(3), O1− −0.05(3), O2+ −0.02(3), O2− −0.08(4), O3+ 0.17(4), O3− −0.02(4), κ(M1) 1.09(2), κ(mul) 0.75(5)
D(1): M1 0.99(9), D0 0.36(5), D1+ −0.02(4), D1− 0.07(5), Q0 0.23(7), Q1+ 0.03(5), Q1− 0.07(5), Q2+ 0.02(5), Q2− 0.00(5), κ(M1) 0.94(3), κ(mul) 1.00(5)
D(2): M1 1.10(10), D0 0.40(6), D1+ −0.02(4), D1− 0.11(4), Q0 0.27(7), Q1+ 0.07(6), Q1− 0.07(6), Q2+ −0.00(5), Q2− −0.01(4), κ(M1) 0.94(3), κ(mul) 1.00(5)
D(3): M1 1.13(10), D0 0.42(6), D1+ −0.04(4), D1− 0.02(4), Q0 0.20(7), Q1+ 0.06(5), Q1− 0.01(5), Q2+ 0.00(4), Q2− 0.07(5), κ(M1) 0.94(3), κ(mul) 1.00(5)

Table 2 Refinement residuals for the XD multipole model

N_o	N_v	R_F	R_{wF}	R_{F^2}	R_{wF^2}	Goodness of fit
4006	140	0.0234	0.0273	0.0303	0.0539	1.257

deuteriums. The model contained an isotropic extinction parameter (type I, Becker and Coppens,[17] Lorentzian distribution) and two scale factors, the last because the data set consists of two blocks collected slightly separated in time (see ref. 6). In all refinements full-matrix least-squares minimisation was used. The maximum shift/e.s.d. was less than 0.005 and the maximum amount of extinction is for the 001 reflection ($y = 0.67$) with only 11 other reflections having more than 10% extinction. The refinement was constrained to maintain overall electroneutrality of the unit cell. No other constraints were introduced besides those mentioned above and those imposed by the choices of the local coordinate systems.§ For all non-deuterium atoms both the core and the valence scattering function were calculated from Hartree–Fock atomic wavefunctions.[18] For the nickel site, functions for Ni^0 were used with the radial form of the valence functions derived from 3d atomic orbital products for the contracted set of functions and from 4s orbital products for the diffuse set of functions. For deuterium the scattering factors calculated by Stewart *et al.*[19] were used.

A number of other models were tested before deciding on the above model. For instance we tried to refine separate κ parameters for all multipole orders on all atoms. While such refinements achieve convergence they do not improve the residuals nor lead to differences in the topological features discussed below. The extra κ parameters were therefore deemed unimportant. Only for N(1) the use of separate κ parameters for each multipole order was found to be important for the topology of the static model density. Fourth-order multipoles were tested on the N and O atoms, but were found to refine to insignificant values and were therefore omitted. Introduction of anharmonic thermal parameters was also tried on all atoms, but none of them refined to significant values. The study therefore shows that anharmonic motion appears to be negligible at temperatures close to absolute zero.

§ The following local coordinate systems were adapted: Ni [*Z* axis Ni ⟶ (0, 1, 0), *X* axis Ni ⟶ N(1)], O(1) [*Z* axis O(1) ⟶ (0.3082, 1, 0.1924), *X* axis O(1) ⟶ N(1)], O(2) [*Z* axis O(2) ⟶ (0.2135, 1, −0.2096), *X* axis O(2) ⟶ N(1)], N(1) [*Z* axis N(1) ⟶ (0.2005, 1, −0.0063), *X* axis N(1) ⟶ Ni], N(2) [*Z* axis N(2) ⟶ Ni, *X* axis N(2) ⟶ (−0.0164, 0.3098, 0.2573)], D(1) [*Z* axis D(1) ⟶ N(2), *X* axis D(1) ⟶ (1, 0, 1)], D(2) [*Z* axis D(2) ⟶ N(2), *X* axis D(2) ⟶ (1, 0, 1)], D(3) [*Z* axis D(3) ⟶ N(2), *X* axis D(3) ⟶ (1, 0, 1)].

In Fig. 2 residual maps are shown for two sections through the molecule. In general the residual features are less than 0.2 e $Å^{-3}$. The small peak relatively near the nickel atom in the Ni–N(1)–O(2) plane could not be modelled even with use of the extra parameters described above. It may be due to a small systematic error in the data. In Table 1 the refined electron-density parameters are listed, and in Table 2 refinement residuals for the XD multipole model are shown. The positional and thermal parameters were given in ref. 6.

The monopole populations obtained from more restricted multipole refinements have in many previous studies been used to assign pseudo-atom charges.[20] However, when using a diffuse and necessarily flexible model such assignments are not meaningful. In the present model it is especially the Ni- and the ligating nitrogen-centred functions which are very diffuse. This leads to unrealistic charges. Indeed the pseudo-atom monopole populations suggest a negative nickel atom. At the end of the paper we will briefly discuss simplified and less diffuse models which qualitatively give 'better' pseudo-atom charge assignments. However such models are no longer adequate for detailed description of the data. Therefore quantitative discussions of the atoms in the molecule are in this paper carried out by analysis of the total electron density using rigorous topological methods.

Theoretical Calculations

For comparison with the experimental ammonia and nitrite critical point analysis and deformation density we calculated good-quality wavefunctions for the free ammonia molecule and for the nitrite ion. Since our objective is to examine any changes due to bonding in molecule **2**, we require calculations which are chemically indistinguishable from exact results. Accordingly we followed the prescription of Schaefer *et al.*[21] Using their triple-zeta plus two polarisation function Gaussian basis set (TZ2P) we optimised the nuclear geometry in the Hartree–Fock framework using the *ab-initio* package GAMESS[22] implemented on a DEC alpha workstation with 8 Gbyte disk storage. The resulting energies and geometries are: NH_3, $E = -56.220\ 26$ au, $r(N-H) = 0.9980$ Å, $\theta(H-N-H) = 107.8°$; NO_2^-, $E = -204.154\ 68$ au, $r(N-O) = 1.2208$ Å, $\theta(O-N-O) = 116.9°$. At this geometry we introduced configuration interaction, using all single and double excitations (29 161 configurations in Cl sym-

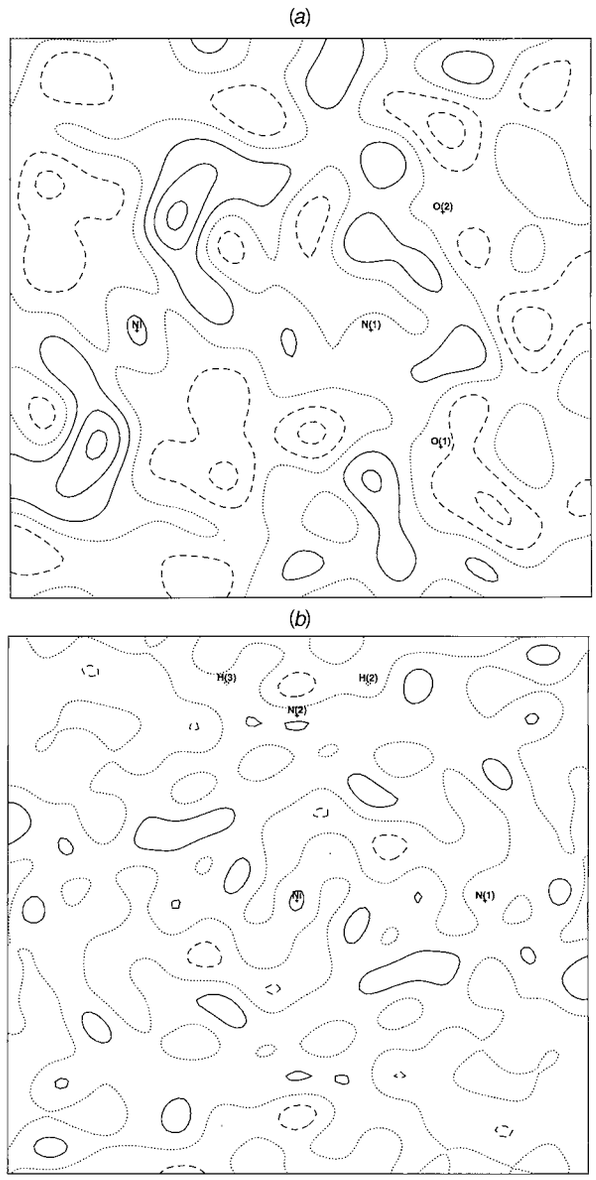

Fig. 2 Residual density in the Ni–N(1)–O(2) plane (*a*) and in the Ni–N(1)–N(2) plane (*b*). The resolution of the maps is 0.8 $Å^{-1}$ and the contour interval is 0.1 e $Å^{-3}$. Solid lines represent positive contours and broken lines negative contours

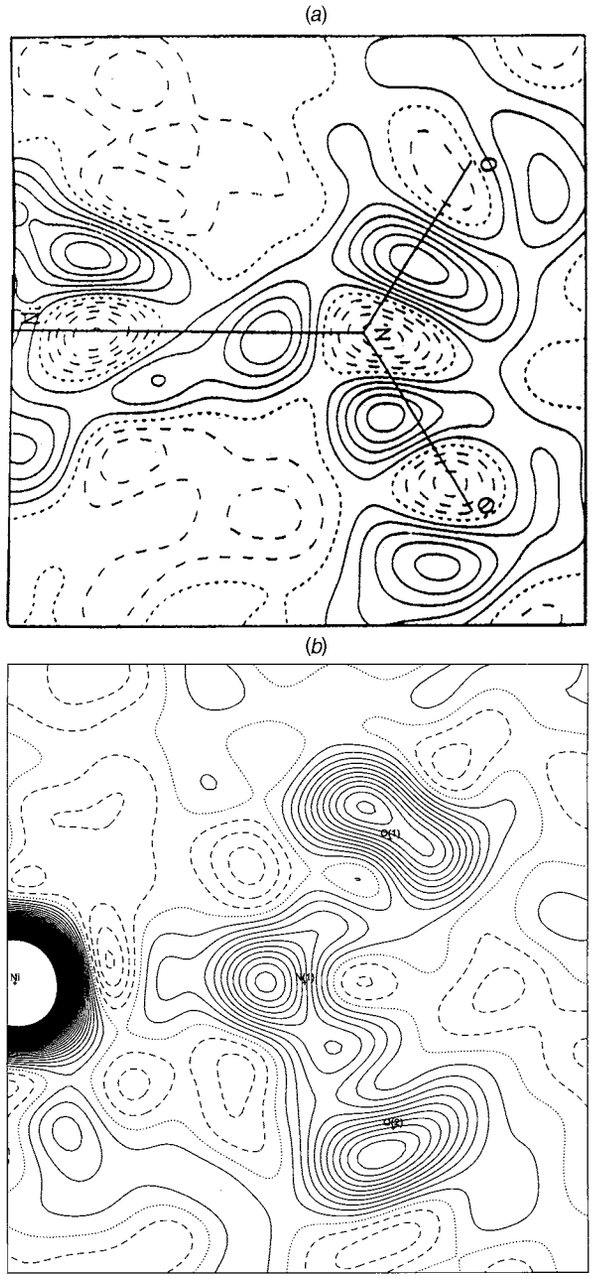

Fig. 3 Experimental deformation densities in the Ni–N(1)–O(2) plane: (*a*) copied from Figgis *et al.*,[9c] (*b*) present study. Contours and resolution as for Fig. 2

metry for NH_3 and 314 821 in Cl symmetry for NO_2^-) giving final energies of −56.455 73 and −204.751 38 au. This calculation duplicates that for NH_3 of Schaefer *et al.*[21] so that appropriate properties of the wavefunction can be derived. That for NO_2^- is an improvement on earlier studies[23] which used at best only double zeta plus single polarisation, included no electron correlation and reached a lowest energy of −204.1318 au. We also carried out the same calculations at the experimental geometry. For NH_3 the results are almost unchanged and only the optimised geometry results are discussed.

Deformation densities

The improvement in the 9 K data over the 110 K data is immediately visible when mapping the difference between observed and spherical atom model densities, Fig. 3. Compared to the 110 K data of Figgis *et al.*[9c] the 9 K data reach much higher contour levels, mainly because of less thermal motion.

In Fig. 4 dynamic model deformation maps are shown. Holes in the 3d-like distribution along the six nickel–ligand bonds are observed as predicted by the crystal-field model for a Ni^{2+} ion in tetragonal symmetry. The holes directed towards the ammonia groups are deeper than the holes towards the nitrite groups. Lone pairs as well as bonding densities are clearly visible for both the nitrogen and the oxygen atoms. The differences in the crystal environment between the two oxygen atoms are reflected in the model deformation maps. The lone-pair density of O(1), which only accepts two hydrogen bonds, reach a peak height of more than 1.95 e $Å^{-3}$. The lone-pair density of O(2), which is involved in four hydrogen bonds, only reaches 1.50 e $Å^{-3}$. For O(1) a small hole near the nucleus is observed, which for O(2) only is a dip in the positive density.

The qualitative features present in the dynamic model deformation maps are virtually unchanged in the static model deformation maps shown in Fig. 5. If we assume the deconvolution of the thermal motion to be adequate then these maps are directly comparable to theoretical deformation maps. In Fig. 6 deformation maps based on the optimised geometry calculations are shown. The deformation density in the N–H bond resembles that for an uncorrelated TZ1P NH_4^+ calculation,[2] while that for NO_2^- resembles those calculated by Cruickshank

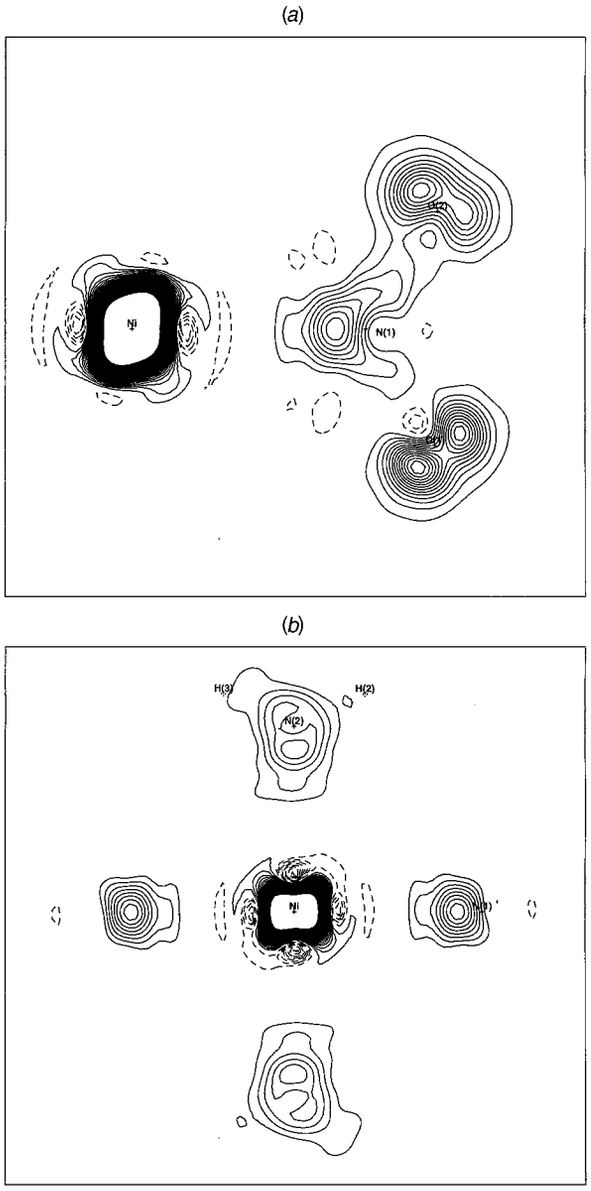

Fig. 4 Dynamic model deformation densities in the Ni–N(1)–O(2) plane (*a*) and the Ni–N(1)–N(2) plane (*b*). The resolution of the maps is 1.4 $Å^{-1}$ and the contour interval is 0.15 e $Å^{-3}$ in order more clearly to illustrate the height of the oxygen lone-pair peaks. Solid lines represent positive contours and broken lines negative contours

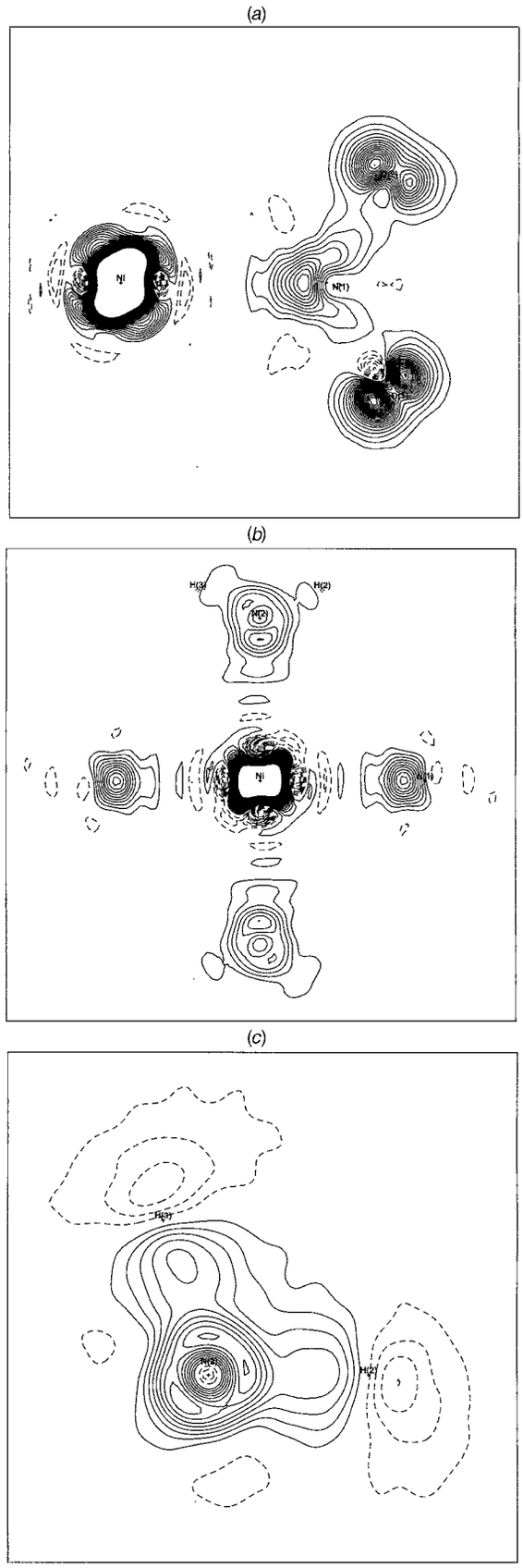

Fig. 5 Static model deformation density in the Ni–N(1)–O(2) plane (*a*), the Ni–N(1)–N(2) plane (*b*), and the N(2)–H(2)–H(3) plane (*c*). For plots (*a*) and (*b*) contours are as for Fig. 4. For (*c*) the contour interval is 0.1 e $Å^{-3}$

and Eisenstein[23b] in DZ1P. They are, however, experimentally distinguishable. For example examination of our maps and those of ref. 23(*b*) shows that our calculation has produced a significant diminution in the hole along the N–O bond from greater than −1.0 to −0.4 e $Å^{-3}$. For compound **1** we have previously shown that triple-zeta calculations do indeed fit X-ray data better than do double-zeta ones.[7]

In the crystal the two N–O bonds are longer than the value obtained by theory. In Fig. 7 the deformation density is shown for a calculation using the experimental geometry. The changes include deeper holes near the oxygens as well as a lowering of the N–O bond peaks. There is good qualitative agreement between the theoretical and the experimental maps, but notable differences are also present. The differences are presumably due to the effect of the crystal environment on the experimental density.

The nitrite ion has been examined in considerable detail both by theoretical methods,[23] but not to a level currently easily obtainable, and by diffraction studies of $NaNO_2$[24] and $K_2NaCo(NO_2)_6$.[25] Deformation maps for the plane containing the N–O bond but perpendicular to the NO_2 plane have been suggested to reveal π-bonding features.[24] In Fig. 8 deformation densities along the N–O bonds in this plane are shown for both the experimentally derived density and for the theoretical calculation employing the optimised geometry. The maps closely resemble the maps obtained for $NaNO_2$ and $K_2NaCo(NO_2)_6$.

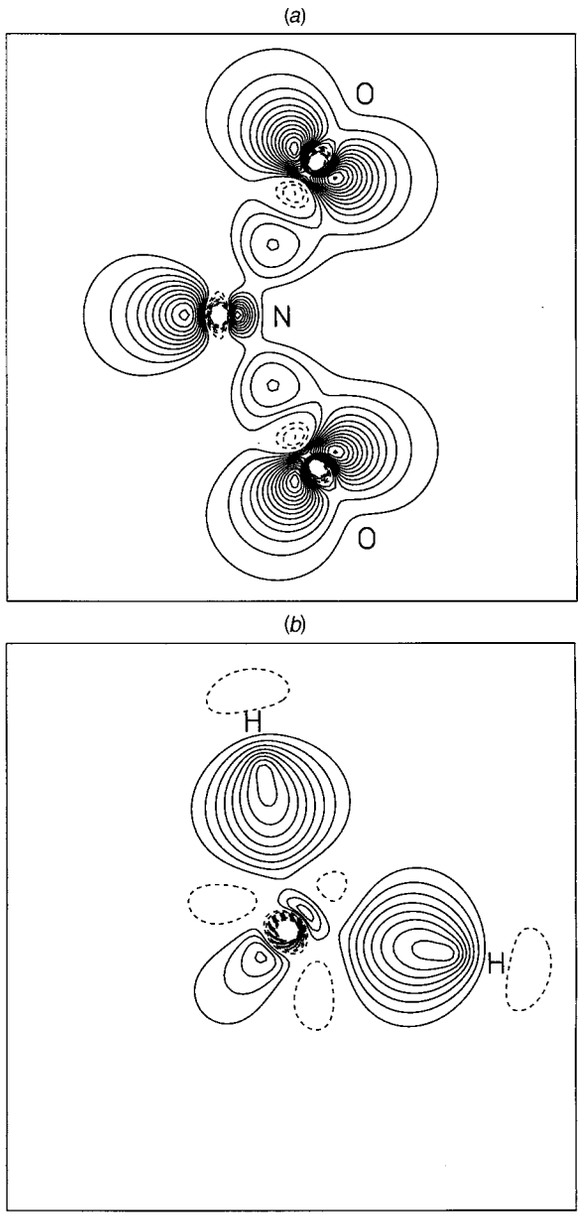

Fig. 6 Static deformation density based on TZDP/CISD calculations at optimised geometry in the O–N–O plane (*a*) and a H–N–H plane (*b*).The contour interval is 0.15 e Å^{-3} in (*a*) and 0.1 e Å^{-3} in (*b*). Solid lines represent positive contours and broken lines negative contours

The differences between the two oxygen atoms due to intermolecular interactions are clearly seen. Since deformation maps are model dependent, conclusions from them about π contributions are ambiguous. Instead, we examine these features below using topological analysis of the total electron density.

The previous theoretical studies of the nitrite ion were particularly concerned with the basis-set dependence of the properties. They showed that polarisation functions are vital in theoretical calculations in order properly to describe bonding effects even for first-row structures. This is confirmed by the present experimental study where we are forced to use third-order multipoles on the O and N atoms in the least-squares fit.

Topology

The topological analysis of electron densities developed by Bader[13] has been extensively presented in the literature. Critical points (CPs) in the density have $\nabla\boldsymbol{\rho} = \mathbf{0}$ and they can in Bader's scheme be classified in terms of the properties of the eigenvalues of the Hessian matrix (second derivatives) at the critical point. The CPs are characterised by (rank, signature) where

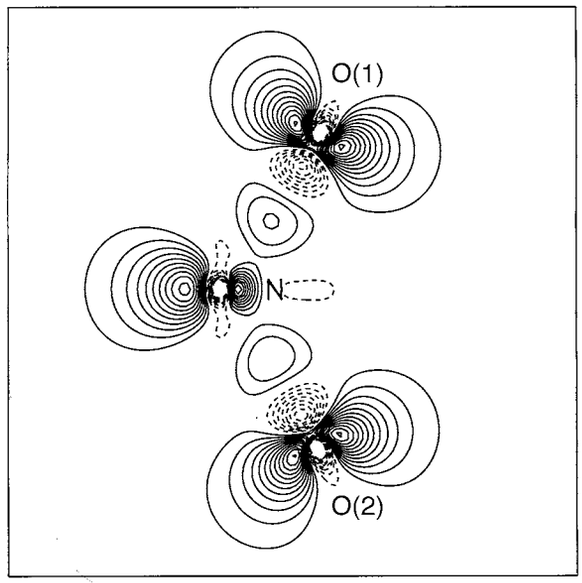

Fig. 7 Static deformation density based on TZDP/CISD calculations at the experimental geometry in the O–N–O plane. Contours as for Fig. 6

rank is the number of non-zero eigenvalues and signature is the algebraic sum of their signs. Atomic entities in the density peak at (3,−3) points and chemical bonds go through (3,−1) points. The (3,1) and (3,3) points define the two other structural concepts, namely rings and cages. Different chemical bonds can be characterised depending on the sign of the Laplacian ($\nabla^2\rho$) at the bond CP. The Laplacian shows where charge is locally concentrated ($\nabla^2\rho < 0$) or depleted ($\nabla^2\rho > 0$). Closed-shell interactions have positive Laplacians (mainly ionic or electrostatic interactions such as hydrogen bonds and van der Waal bonds), whereas electron-sharing interactions have negative Laplacians (covalent bonds). The π character as well as the stability of a bond can be described by the ellipticity of the bond, $\varepsilon = \lambda_1/\lambda_2 - 1$, where λ_1 and λ_2 are the negative eigenvalues of the Hessian matrix at the bond CP.

In Table 3 the bond CPs found in the static model density by the XD program are listed together with values obtained from the theoretical densities (optimised geometry) of NO_2^- and NH_3. Also listed are the eigenvalues of the Hessian matrix, and their sum ($\nabla^2\rho_c$) calculated at the CPs, the lengths of the bond paths and the internuclear distances. The critical points were located as points in the density where the gradient attains a value smaller than 1×10^{-5} e Å^{-4}. The static model density was calculated by including all density functions centred less than 5 Å from the point of consideration. It may be noted that the XD program at present only allows calculation of least-squares error estimates on $\nabla^2\rho_c$ and ρ_c but not on the individual eigenvalues of the Hessian matrix. Such error estimates rely, however, on the adequacy of the model in describing the density. It has recently been shown that even the very flexible models used in experimental EDD analysis do not fully exhaust the information in the data,[7] and that the radial form of the fitting functions is important for the fine details of the model density. It is probably therefore a fairer estimate of the uncertainty in the topological features derived from experimental data to state the values obtained with different models having very similar values of χ^2. In the discussion below we state the values obtained with different models whenever there is a notable difference.

The nitrite ion

Results of the topological analysis of the nitrite group are shown in Fig. 9 and in Table 3. The first two bond CPs listed in

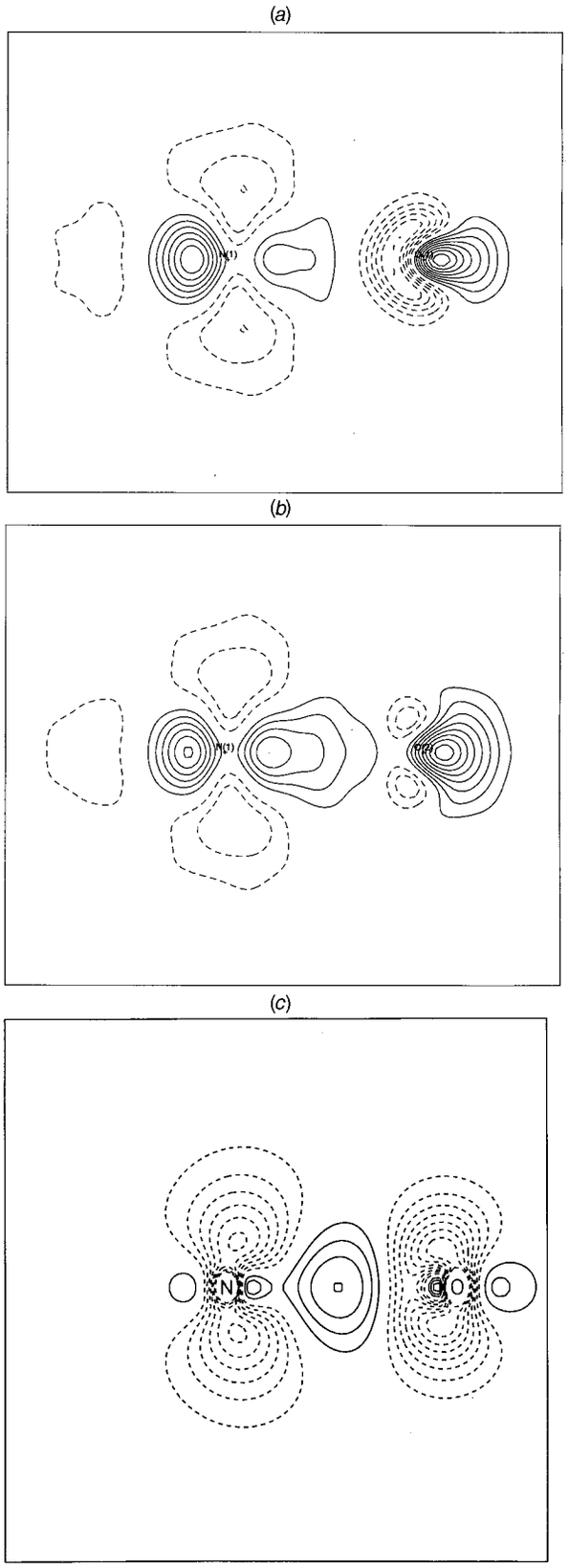

Fig. 8 Static model deformation density along the N(1)–O(1) bond (*a*) and the N(1)–O(2) bond (*b*) in the plane perpendicular to the molecular plane. In (*c*) the same plane is shown for the TZDP/CISD calculations employing the optimised geometry. The contour level is 0.15 e Å^{-3}. Solid lines represent positive contours and broken lines negative contours

Table 3 correspond to the N–O bonds of the nitrite group. It is striking that both ρ_c, $\nabla^2\rho_c$ and the individual values of the Hessian matrix are so similar for the two bonds, when considering the differences found in the experimental deformation density. The fact that the two N–O bonds appear topologically equivalent suggests that the effect of the crystal environment is confined to the lone-pair regions and to near the oxygen nuclei. In the N–O bonds $\nabla^2\rho_c$ is large and negative as expected for a covalent-type interaction. If we do not use extra radial flexibility in the modelling of N(1) the values of ρ_c drop to 3.18 and 3.26 e Å^{-3} for the N(1)–O(1) and N(1)–O(2) bonds respectively; $\nabla^2\rho_c$ grows to −3.7 and −3.4 e Å^{-5}. Since we expect a large degree of covalency in the nitrite bonds we deemed the extra radial flexibility important, even though it only gives a very slight improvement in the refinement residual. The large numerical increase in $\nabla^2\rho_c$ when introducing extra radial flexibility is both due to a smaller positive curvature and larger negative curvatures at the bond critical points. In general the positive curvature is especially sensitive to the radial form of the fitting functions. Recently Bianchi *et al.*[26] studied lithium bis(tetramethylammonium) hexanitrocobaltate(III) using both theoretical methods and multipole modelling of 100 K X-ray diffraction data. In this study ρ_c in the N–O bonds are 3.19(4) and 3.44(4) e Å^{-3} for the experimental density, and 3.28 and 3.39 e Å^{-3} for the theoretical calculations employing the Hartree–Fock periodic approach.[27] For $\nabla^2\rho_c$ Bianchi *et al.*[26] obtained −7.5 and −11.9 e Å^{-5}. When comparing the experimental Laplacians to theory it is clear that theory gives a smaller value of the positive curvature than does the multipole analysis. Since the effect of employing separate κ values on N(1) was to lower the value of the positive curvature, comparison between theory and experiment indicates that even the radially flexible model used in this study may still be too rigid. A simple Lewis electron-pair model predicts for a NO_2^- ion that the N–O bond is intermediate between a single and a double bond. In other words, π contributions to the bonding are expected. The π contributions are reflected in the non-cylindrical shape of the electron density at the bond critical points. The ellipticity at the bond CP measures this shape and we obtain values of 0.15 and 0.12 for the two N–O bonds respectively. The ellipticity of the bonds is also affected by the extra κ parameters on N(1) [0.06 and 0.05 without extra κ parameters on N(1)]. For comparison the ellipticity in carbon–carbon bonds is 0.23 for benzene and 0.45 for ethene.[13] The two bond paths between the N and O nuclei fall almost exactly on the internuclear axis as seen in the identical values of R_{ij} and D_{ij}. Figgis *et al.*[9b] noted that the difference in the number of hydrogen bonds to the two oxygen atoms presumably causes the observed difference in the N–O internuclear distance [1.244(1) and 1.255(1) Å]. The bond critical point is almost exactly at the same distance from the nitrogen atom in the two N–O bonds. This means that the difference mainly resides inside the atomic basins of the oxygen atoms.

The ammonia molecule

Results of the topological analysis of the ammonia molecule are shown in Figs. 10 and 11 and in Table 3. For the ammonia molecule the densities at the bond CPs are smaller than for the nitrite ion. They are in good agreement with values found in other studies of N–H bonds.[13,14a,e28] The three N–D bonds have similar values of ρ_c. This need not be so since each deuterium atom is also involved in hydrogen bonding in which charge migration takes place. For all three bonds very large and negative values of the Laplacian are obtained indicating a large degree of covalency in the bonds. If we introduce additional flexibility through use of separate κ parameters on each multipole order on N(2) the values of $\nabla^2\rho_c$ are −88.8, −56.5 and −51.2 e Å^{-5} for the three N–D bonds respectively. The values of $\nabla^2\rho_c$ are somewhat larger than those reported in the literature.[13,14a,c] When examining the values of the Hessian matrix it is clear that it is the positive eigenvalue, especially, which is smaller in the present study. The positive eigenvalue reflects movement of charge away from the bond CP and into the atomic basins. As explained above it is intimately related to

Table 3 Bond critical points in the static XD model density: the first entry is the experimental density, the second the theoretical density; ρ_c (e Å^{-3}) is the electron density, $\nabla^2\rho_c$ (e Å^{-5}) the Laplacian at the CP, λ_1, λ_2, λ_3 (e Å^{-5}) are the eigenvalues of the Hessian matrix, ε is the ellipticity, d_1 and d_2 are the distances to the bond path attractors, R_{ij} (Å) is the sum of d_1 and d_2 and D_{ij} (Å) is the internuclear distance as obtained from the neutron diffraction data

	ρ_c	$\nabla^2\rho_c$	λ_1	λ_2	λ_3	ε	R_{ij}	d_1	d_2	D_{ij}
N(1)–O(1)	3.57(7)	−18.6(3)	−37.1	−32.2	50.7	0.15	1.24	0.647	0.595	1.244(1)
	3.433	−50	−41	−28	19	0.46		0.665	0.563	
N(1)–O(2)	3.61(7)	−17.8(3)	−37.5	−33.4	53.1	0.12	1.26	0.649	0.609	1.255(1)
	3.433	−50	−41	−28	19	0.46		0.665	0.563	
N(2)–H(1)	2.10(1)	−69.2(6)	−39.6	−39.0	9.5	0.01	1.02	0.859	0.158	1.015(1)
N(2)–H(2)	2.403	−40	−30	−30	20	0		0.730	0.267	
	2.13(1)	−54.3(5)	−33.9	−33.2	12.8	0.02	1.01	0.812	0.198	1.015(1)
	2.403	−40	−30	−30	20	0		0.730	0.267	
N(2)–H(3)	2.21(1)	−53.5(6)	−33.9	−32.1	12.5	0.06	1.01	0.806	0.205	1.014(1)
	2.403	−40	−30	−30	20	0		0.730	0.267	
Ni–N(1)	0.65(2)	7.1(2)	−3.4	−2.3	12.8	0.45	2.15	1.046	1.099	2.142(1)
Ni–N(2)	0.76(5)	9.9(3)	−3.0	−2.9	15.8	0.04	2.11	0.010	1.101	2.106(1)
N(2)–D(1) ··· O(2)	0.10(2)	0.56(3)	−0.5	−0.5	1.5	0.07	2.19	0.841	0.354	2.175(1)
N(2)–D(2) ··· O(2)	0.12(2)	0.45(3)	−0.7	−0.6	1.7	0.10	2.14	0.815	1.328	2.126(1)
N(2)–D(3) ··· O(1)	0.09(2)	0.71(3)	−0.5	−0.4	1.6	0.27	2.19	0.842	1.353	2.159(1)

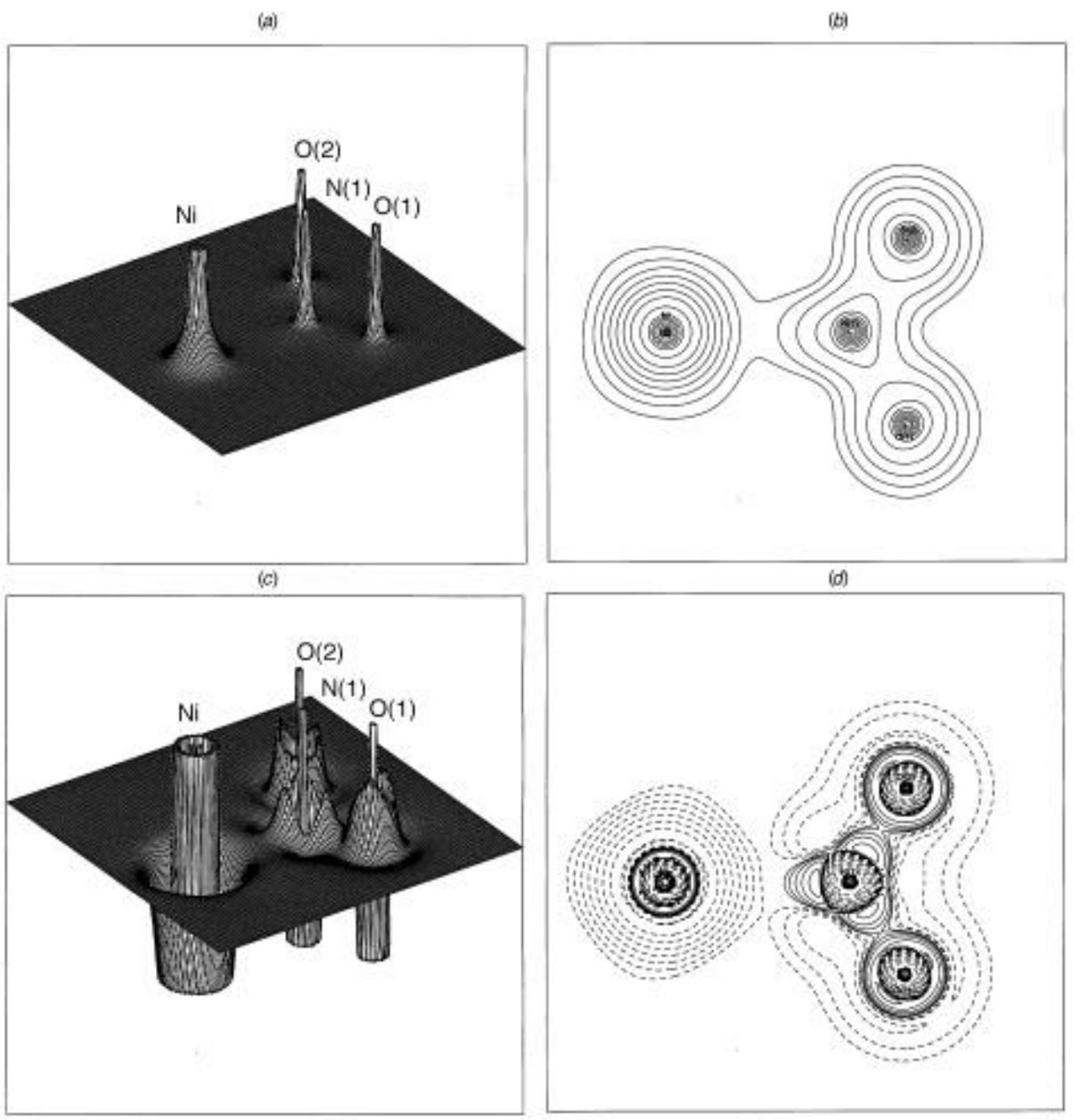

Fig. 9 Plots of the total static model electron density (ρ), and the negative Laplacian of the total static model electron density ($-\nabla^2\rho$) in the nickel–nitrite plane. (*a*) Relief plot of ρ. The density is truncated at 256 e Å^{-3}. (*b*) Contour plot of ρ. The contours are drawn on a logarithmic scale, 1.0×2^N e Å^{-3}. (*c*) Relief plot of $-\nabla^2\rho$. Negative and positive regions are truncated at −256 and 256 e Å^{-5}. (*d*) Contour plot of $-\nabla^2\rho$. The contours are drawn on a logarithmic scale, 4.0×2^N e Å^{-5}

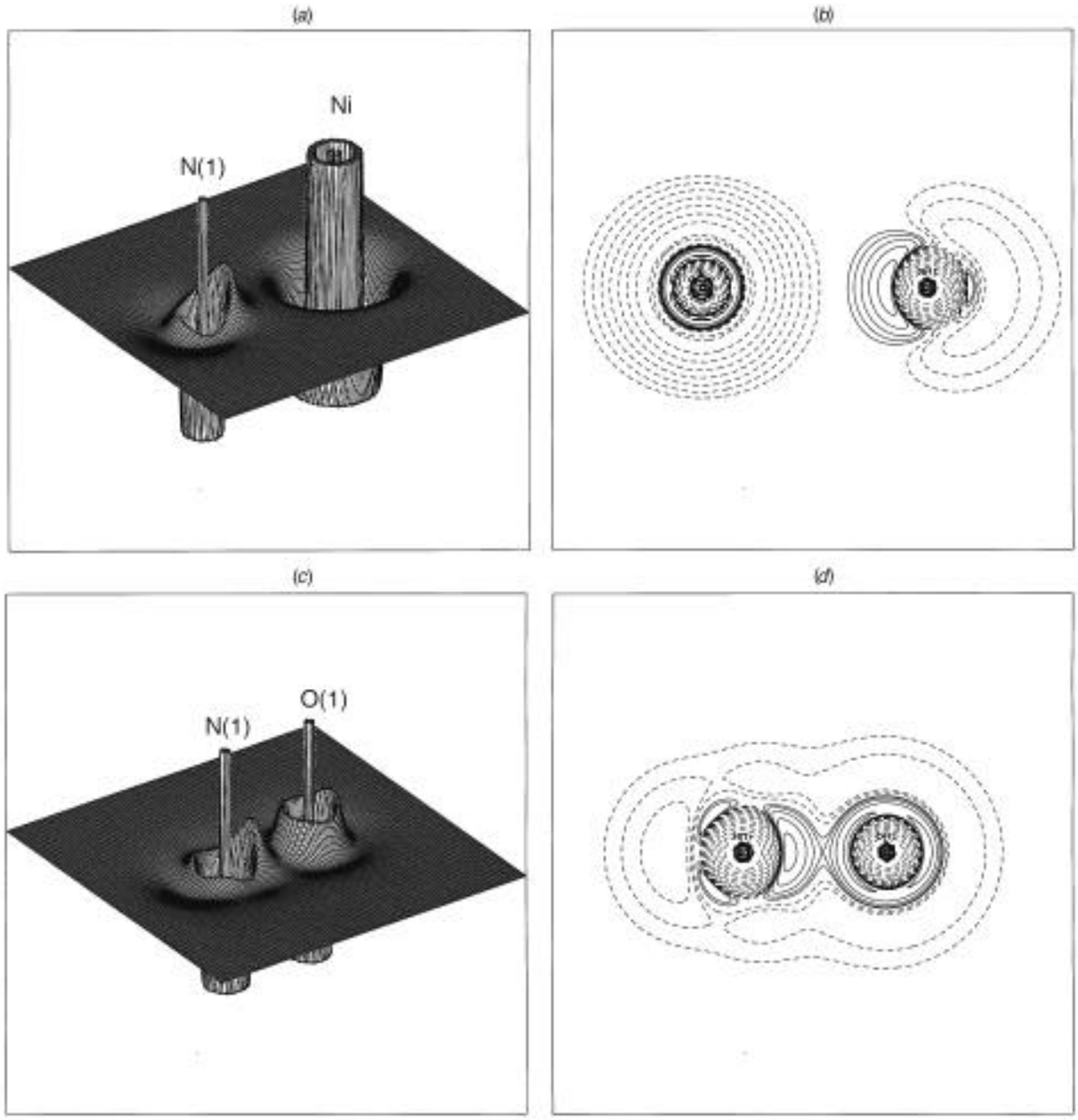

Fig. 10 Plots of $-\nabla^2\rho$ for the nitrite ion based on the total static model density. (*a*) Relief plot in the Ni–N(1) plane perpendicular to the molecular plane. Truncation as in Fig. 9(*c*). (*b*) Contour plot of the Ni–N(1) plane. Contour interval as in Fig. 9(*d*). (*c*) Relief plot in the N(1)–O(1) plane perpendicular to the molecular plane. Truncation as in Fig. 9(*c*). (*d*) Contour plot of the N(1)–O(1) plane. Contour interval as in Fig. 9(*d*)

the radial form of the density functions. It should again be stressed that the present study employs more radial flexibility than is normally used in experimental charge-density studies, and we also have an unusually precise deconvolution of the thermal motion. We are therefore inclined to believe in the larger negative values found for ND_3.

As expected the shapes of the electron density at the N–D bond CPs are almost cylindrical, which is reflected in the small bond ellipticities (0.01, 0.02 and 0.06). These values are unaffected by introduction of extra radial flexibility on the ammine group. The bond paths are close to the internuclear axis as seen in the equal values of R_{ij} and D_{ij}. Figgis *et al.*[9b] observed a weak band at 1850 cm^{-1} in the IR spectrum which they assigned to a weaker N–D(1) bond compared to N–D(2) and N–D(3). The monopole population on D(1) is somewhat smaller than the corresponding D(2) and D(3) monopole populations, and ρ_c is slightly smaller for N–D(1) than for N–D(2) and N–D(3). On the other hand the Laplacian shows, if anything, a more covalent N–D(1) bond. Furthermore, we obtain almost equivalent N–D internuclear distances. Also the O ··· D distances are almost equivalent. The geometries of the hydrogen bonds are slightly different; for D(2) and D(3) the N–D ··· O angle is close to 180° [179.1(1) and 175.4(1)] compared to 165.9(1)° for D(1). The value of ρ_c is very similar for all three hydrogen bonds which have small positive values of the Laplacian at the bond CP reflecting closed-shell interactions. For all three bonds the bond paths follow the internuclear axis with R_{ij} being only about 0.01–0.03 Å longer than the internuclear separation. In conclusion the topological analysis is not conclusive about the proposed weakening of N–D(1). The band at 1850 cm^{-1} in the IR spectrum may have another origin.

Metal–ligand interaction

The topological analysis shows that both the nitrite ion and the ammonia ligands have positive Laplacians at the metal–ligand bond CP. These values are positive irrespective of the choice of model. Thus both ligand types are co-ordinated to nickel in predominantly ionic interactions. Figgis *et al.*[9c] showed that the crystal-field model is a reasonable first approximation to

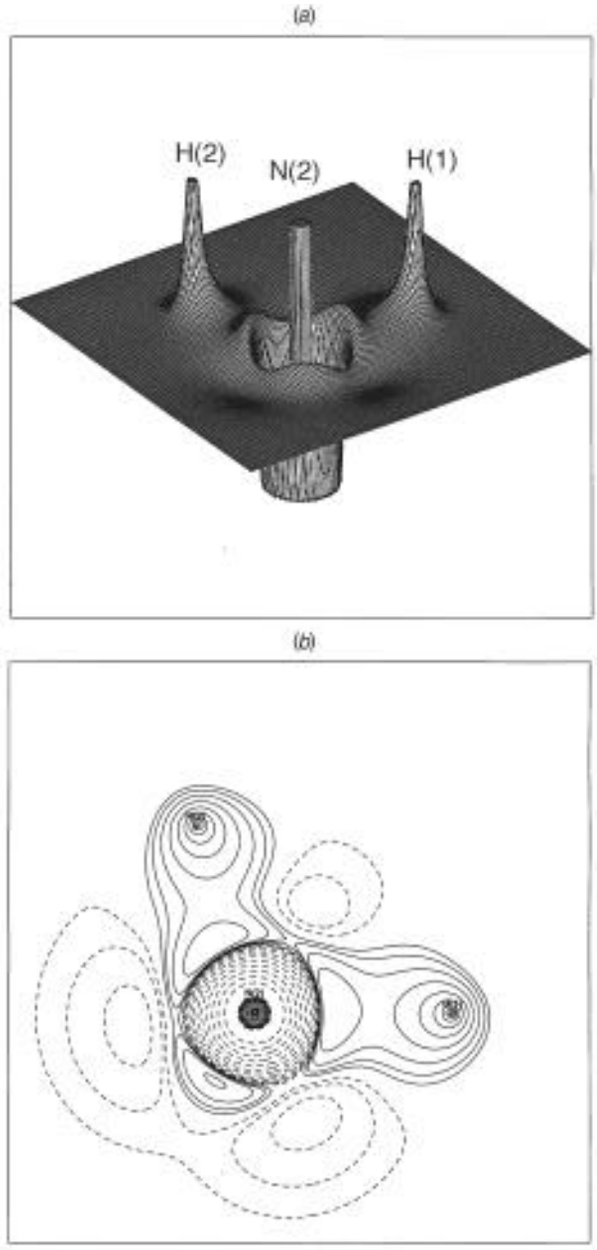

Fig. 11 Plots of $-\nabla^2\rho$ for the ammonia molecule in the N(2)–H(1)–H(2) plane. (*a*) Relief plot with truncation as in Fig. 9(*c*). (*b*) Contour plot with contour interval as in Fig. 9(*d*)

describe the bonding in compound **2** at a qualitative level. This is faithfully mapped in the Laplacian of the density. In all models the nickel–ammine bond consistently has a larger positive value of the Laplacian compared to the nickel–nitrite bond. This indicates that the nitrite ligand has a greater degree of covalency in the bond compared to the nickel–ammine bond, as expected from the relative positions of the ligands in the spectrochemical series.

In the previous 110 K study Figgis *et al.*[9c] found that the nitrite ligand is a stronger σ donor than the ammonia ligand. No evidence was found for a π contribution to the metal–ligand bonding for either the nickel–nitrite or –ammine bond. In that study a valence-orbital model gave an adequate description of the data, but as will be shown below it is not adequate in the description of the more accurate less thermally affected 9 K data. There is a clear difference between the ellipticities in the two metal–ligand bonds. The nickel–nitrite bond has an ellipticity of 0.45 whereas the nickel–ammine bond only shows weak ellipticity (ε = 0.04). For the nitrite bond the ellipticity is perpendicular to the mirror plane. Even though there is some uncertainty about the exact values of the ellipticities, this study suggests that π interaction takes place in the nickel–nitrite bond, which may be regarded as having a π as well as a σ component in the covalent part. The ammine ligand is mostly bonded through σ interaction for the covalent part of the bonding. This conforms with the conventional ligand-field angular-overlap-model contention that primary amine ligand bonding to metals does not contain a π component. If we omit the extra radial flexibility on N(1) the ellipticity in the nickel–nitrite bond drops to 0.06.

In the simple ligand-field picture we expect π-back donation from the nickel ion into the π* antibonding orbital of the nitrite group since we are formally dealing with an electron-rich 20-electron complex. The archetype examples of metal to ligand π-back donation are carbonyl complexes. Evidence for π-back bonding has earlier been given based on deformation densities in a study of $[Cr(CO)_6]$.[29] Furthermore a large amount of *indirect* evidence has accumulated supporting the idea of π-back donation in the bonding. Among this indirect evidence is the observed lowering of the CO stretching frequencies in the IR spectrum.[30] Other evidence includes the fact that the CO internuclear distance is increased by 0.01–0.06 Å for co-ordinated carbonyls compared to free CO.[31] However, unlike considerations about the internuclear distances, the topological evidence is a direct experimental validation of the π-back-donation scheme, which is a generally accepted simple bonding model for transition-metal complexes.

Laplacian of the Electron Density

In the preceeding paragraph it was shown that the values of the second derivatives of ρ can be used to describe chemical bonding in transition-metal complexes. In general the Laplacian shows where charge is locally concentrated ($\nabla^2\rho < 0$) or depleted ($\nabla^2\rho > 0$). This is in contrast to the total density which is a smoothly decaying function away from the nuclei. In Fig. 9 plots of ρ and $-\nabla^2\rho$ are shown for the nickel–nitrite plane. Note that the negative of the Laplacian, $-\nabla^2\rho$, is plotted in order that positive regions correspond to regions of charge concentration.

Atoms in molecules have a shell structure of alternating charge concentrations and charge depletions corresponding to the quantum shells. This shell structure is seen as positive and negative spikes in $-\nabla^2\rho$. The outermost region of charge concentration has been termed the valence-shell charge concentration (VSCC).[13] It has been shown that the maxima in the VSCC correspond in number and positions to the electron pairs of the Lewis model.[31] The local maxima in our experimental VSCC are clearly seen in Fig. 9. For the oxygen atoms there are maxima in the bond directions and for lone-pair charge concentrations. If we map the Laplacian in the plane perpendicular to the mirror plane we observe new features of the VSCC for the nitrite group atoms. In Fig. 10 maps of the negative of the Laplacian for the Ni–N(1) and N(1)–O(1) bonds perpendicular to the molecular plane are shown. While the oxygen atom clearly has strong charge concentrations in all directions, the nitrogen atom shows much more structure in the VSCC. For the nitrogen atom there are clear regions in charge depletion in the valence shell. The regions of charge depletion in the VSCC of N(1) confirm the simple view of the nitrite group with a 'negative' oxygen and a 'positive' nitrogen. The Ni atom shows even greater charge depletion in the valence shell, and it appears totally stripped for its outer charge concentration. This corroborates the expectation of a nickel ion which has lost the 4s electrons.

In Fig. 11 the negative of the Laplacian is plotted for a section through the ND_3 group. Again the VSCC faithfully shows the charge concentrations expected in the N–D bonds. The nitrogen atom in ND_3 has two other maxima in the VSCC besides the ones shown in Fig. 11. These are in the directions of

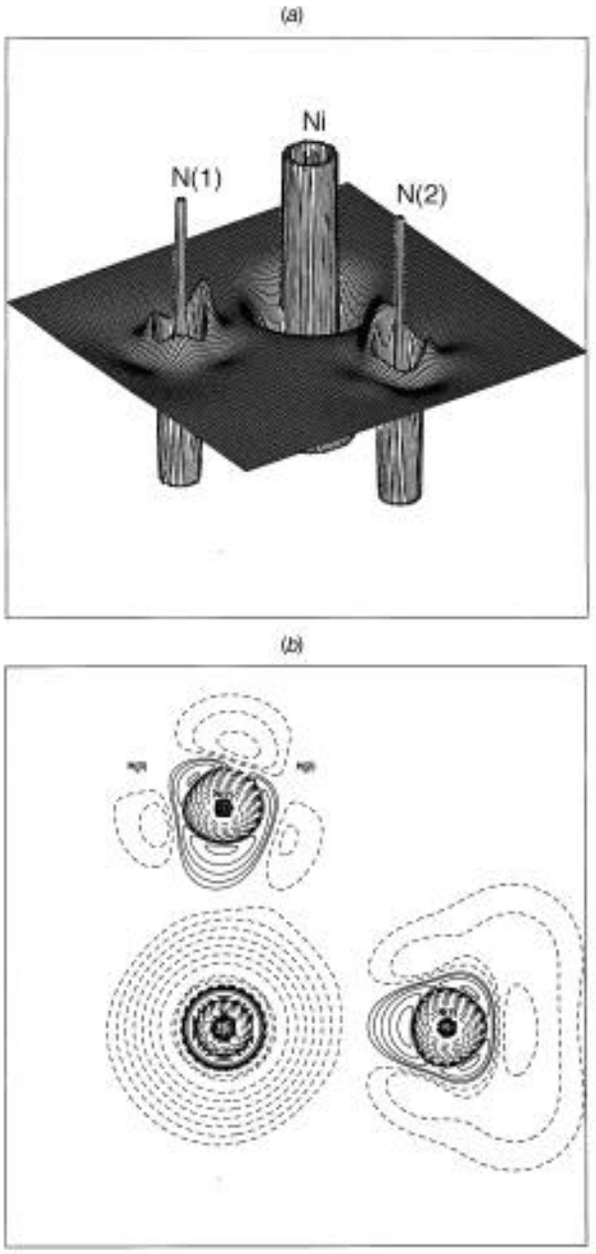

Fig. 12 Plots of $-\nabla^2\rho$ in the Ni–N(1)–N(2) plane. Details as in Fig. 11

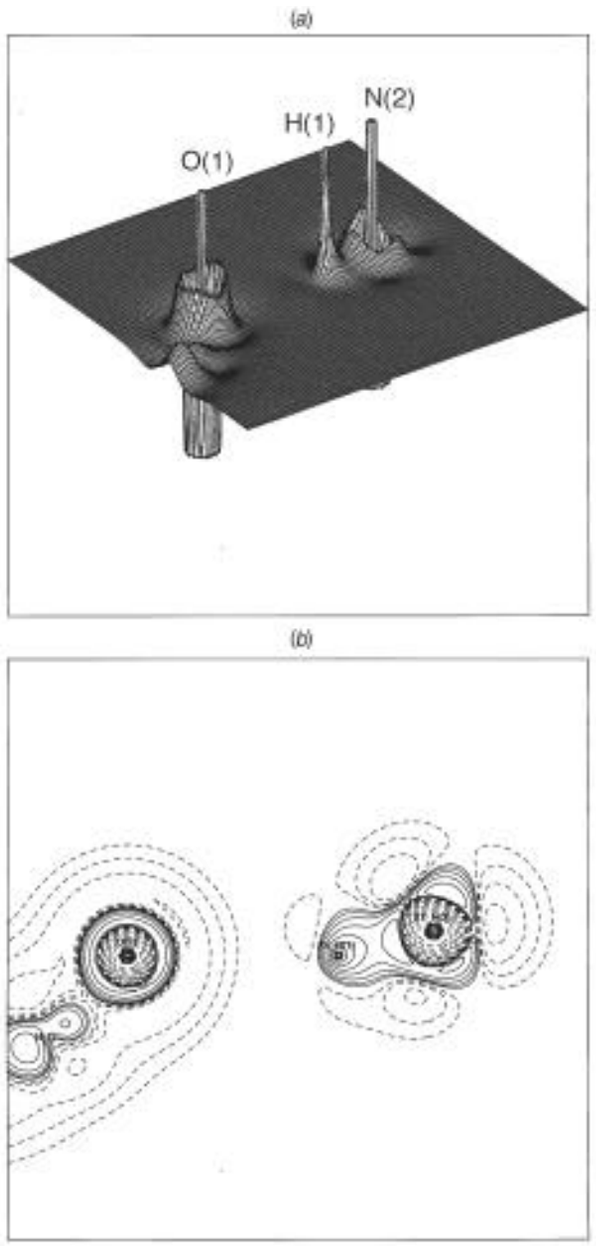

Fig. 13 Plots of $-\nabla^2\rho$ in the O(1) ··· H(1)–N(2) plane. Details as in Fig. 11

Ni and D(1). As can be seen the N–D bonds appear very similar even though the value of the Laplacian is greater in the N–D(1) bond than in N–D(2) and N–D(3). The ammonia group has clear regions of charge depletion on the faces of the $NiND_3$ tetrahedra opposite to the atoms. There are no non-bonded charge concentrations in the VSCC.

In Fig. 12 the negative of the Laplacian is plotted in the Ni–N(1)–N(2) plane. In this plot both the donating nitrogen lone pairs are clearly seen.

The hydrogen-bond interactions are also reflected in the VSCC of the atoms. In Fig. 13 the negative of the Laplacian is plotted for the representative N(2)–H(1) ··· O(1) plane. A small maximum in the VSCC of O(1) is seen in the direction of the hydrogen atom. The numerical value of the Laplacian is relatively small in the hydrogen-bonding region. The important point is that the interaction can be classified as a normal hydrogen bond. Recent topological analyses of small organic molecules with very short intramolecular hydrogen bonds have shown that in special cases the interaction can change character and become predominantly covalent if the O ··· H distance is sufficiently short.[14c,f]

Valence Orbital Models

The topological analysis presented above was based on a very flexible electron-density model. Such a model is necessary in order to exhaust the information in the data. With the flexible model only the total electron density is well modelled, and atomic properties can be derived only through topological analysis. Conventionally, more restricted models are used in experimental charge-density analysis. Restricted models allow better pseudo-atom properties such as orbital populations to be derived, but at the expense of only being semiquantitative. The most chemically inspired restricted model is the valence-orbital model advanced by Figgis *et al.*[32] In order to get a qualitative, but also more chemically intuitive, understanding of the chemistry in the complex in conventional terms, we have also refined various valence-orbital models. The valence-orbital approach can be viewed as a restricted multipole refinement where the fitting functions are limited to those deemed important based on chemical intuition. For a discussion of different electron-density modelling techniques readers are referred to our paper on compound **1**.[2]

In the valence-orbital refinements the program ASRED[30]

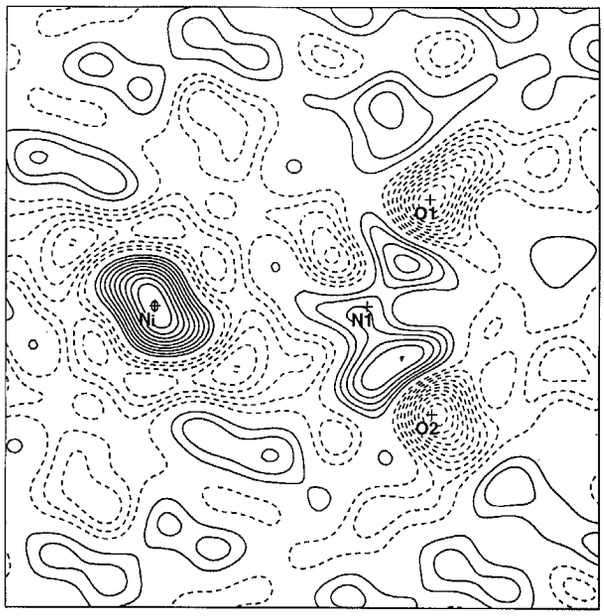

Fig. 14 Residual density in the Ni–N(1)–O(1) plane based on the valence-orbital model and including all data in the refinement. The resolution of the map is 0.8 $Å^{-1}$ and the contour interval is 0.1 e $Å^{-3}$. Solid lines represent positive contours and broken lines negative contours

was used. This minimises the function $\Sigma w(I^{obs} - I^{calc})^2$ where $w = 1/\sigma^2(I)$. Initially we refined a model similar to the aspherical valence model of the 110 K X-ray study[9c] using only the new 9(1) K X-ray data. This allows direct comparison with the results obtained at 110 K and thus demonstrates the advantages of doing crystallography at very low temperatures. The model contained, besides two scale factors, positional and anisotropic thermal parameters on all atoms except for deuterium where isotropic thermal parameters were used. Corrections were made for type II extinction[17] and for multiple scattering by a two-parameter function.[33] Furthermore the cell content was constrained to the correct number of electrons (228.6). The electron-density model included core, 3d and 4p functions on Ni, cores, three sp^2 hybrids and one p_π function on O(1), O(2) and N(1), core and four sp^3 hybrid functions on N(2) and deuterium 1s functions. For all heavy atoms a radial κ parameter was refined for the valence shell. The local atomic coordinate systems were chosen as in the 110 K study. The d orbitals on the nickel atom are labelled according to the Cartesian axis system appropriate to the molecular point group, $x||b$, $y||c^*$, $z||a$. Note that this is not the 'natural' octahedral system, and our axis system gives d_{xy} and d_{z^2} not $d_{x^2-y^2}$ and d_{z^2} as the octahedral e_g set. The refinement results are summarised in Table 4. Scattering factors were calculated for core and valence functions from the atomic wavefunctions of Clementi and Roetti[18] using the program JCALC.[34]

The valence-orbital model provides, contrary to the 110 K study, a quite poor fit to the data and the residual map, Fig. 14, reveals distinct density features which are not fitted by the model. Furthermore many parameters refine to values that are not meaningful. However if we use a cut-off in (sin θ)/λ equal to the resolution of the 110 K study [(sin θ)/λ < 1.08 $Å^{-1}$] much improved residual maps are obtained, Fig. 15. The use of a large amount of accurate high-order data reveals that the valence-orbital model is too rigid to both fit the detailed core information present in the high-order data and describe the reorganisation of charge in the valence regions.

The model is too simple an approximation to separate electronic and vibrational effects properly when very precise information about the thermal motion is present. To demonstrate this even further we compare the values of the thermal parameters obtained with the valence-orbital model refinement to the values from the 13 K time-of-flight neutron diffraction data. The r.m.s. difference between the thermal parameters is $\langle \Delta U^2 \rangle^{\frac{1}{2}} = 0.001\ 14\ Å^2$. This is more than twice that obtained with the very flexible multipole model.

For the valence-orbital refinement with a cut-off in (sin θ)/λ of 1.08 $Å^{-1}$ the pseudo-atom charges are Ni(+1.55), O(1)(−0.40), O(2)(−0.44), N(1)(+0.29), N(2)(−0.48), D(1)(+0.16), D(2)(+0.17) and D(3)(+0.03). These are in good correspondence with what we would qualitatively expect for the system, but as explained above the valence-orbital model does not fully describe the data. With regard to the orbital populations it is clear that the very low $3d_{xz}$ population on Ni obtained by Figgis *et al.*[9c] from 110 K X-ray data is not reproduced by the present more precise data. In general the orbital populations agree better with theory for the 9 K data. It is notable that in all valence-orbital refinements we obtain significantly different

Table 4 Valence-orbital parameters

	Model 1	Model 1 (sin θ)/λ < 1.08	110 K [a]	Theory [b]
N_o	4016 [c]	2083	2109	
N_v	80	80	45 [d]	
R_F (3σ level)	0.0314	0.0173	0.023	
(0σ level)	0.0493	0.0309		
R_{F^2} (0σ level)	0.0722	0.0430	0.035	
Goodness of fit	1.336	0.998	2.1	
Scale factor 1	1.670(6)	1.620(10)		
Scale factor 2	1.461(10)	Not refined		
Ni $3d_{xy}$	1.13(6)	1.09(6)	1.28(7)	1.11
$3d_{xz}$	1.61(6)	1.68(5)	1.31(6)	1.94
$3d_{yz}$	2.02(5)	2.00(5)	1.80(6)	1.99
$3d_{x^2-y^2}$	1.69(6)	1.72(6)	1.84(6)	1.97
$3d_{z^2}$	1.33(5)	1.27(6)	1.36(8)	1.31
$4p_x$	2.1(3)	−0.18(26)	1.59(20)	0.06
$4p_y$	0.4(3)	0.26(23)	0.09(29)	0.04
$4p_z$	−0.6(3)	0.61(27)	−0.19(20)	0.31
κ(3d)	0.99(1)	0.88(2)	1.013(6)	
N(1) p_π	0.24(3)	0.66(6)	0.86(4)	1.07
sp^2(1)	1.25(4)	1.55(5)	1.66(4)	1.70
sp^2(2)	1.12(4)	1.11(5)	1.32(4)	1.17
sp^2(3)	1.46(4)	1.39(5)	1.26(4)	1.17
κ(sp^2)	0.9810(1)	0.96(1)		
N(2) sp^3(1)	0.49(5)	1.50(4)	1.59(3)	1.64
sp^3(2)	0.14(6)	1.33(6)	1.21(3)	1.57
sp^3(3)	0.76(5)	1.33(5)	1.21(3)	1.57
sp^3(4)	0.80(5)	1.32(4)	1.24(3)	1.57
κ(sp^2)	0.9809(1)	1.01(1)	1.052(5)	
O(1) p_π	1.01(6)	1.31(6)	1.61(4)	1.47
sp^2(1)	1.84(4)	1.76(4)	1.61(4) [e]	1.61
sp^2(2)	1.53(4)	1.58(4)	1.43(3)	1.69
sp^2(3)	1.88(4)	1.75(4)	1.62(3)	1.69
κ(sp^2)	0.0795(2)	0.99(1)	1.046(4)	
O(2) p_π	0.98(6)	1.39(6)	1.43(4)	1.47
sp^2(1)	1.84(4)	1.76(4)	1.74(4)	1.61
sp^2(2)	1.59(4)	1.54(4)	1.42(3)	1.69
sp^2(3)	1.84(4)	1.75(4)	1.64(3)	1.69
κ(sp^2)	0.9798(2)	1.00(4)	1.046(4)	
H(1) 1s	1.14(7)	0.84(5)	0.77(4)	0.55
H(2) 1s	1.50(10)	0.83(5)	0.92(3)	0.55
H(3) 1s	3.43(14)	0.97(6)	0.93(3)	0.55

[a] Figgis *et al.*[9c] [b] Chandler *et al.*[7] [c] Ten reflections had negative intensities and were included in the ASRED refinements. [d] Positional and thermal parameters fixed at values from a high-order refinement. [e] pπ orbital.

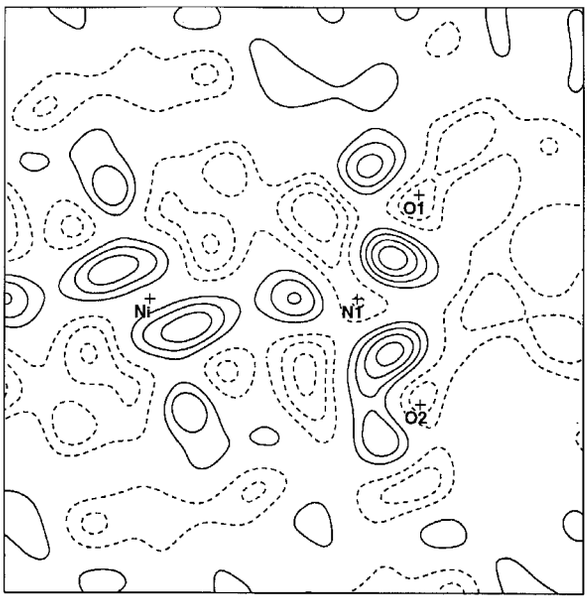

Fig. 15 Residual density in the Ni–N(1)–O(1) plane based on the valence-orbital model and including only data with $(\sin\theta)/\lambda < 1.08$ Å^{-1} in the refinement. The resolution of the map is 0.8 Å^{-1}. Contours as for Fig. 14

values of $3d_{xz}$ compared to $3d_{yz}$. This is in accord with the significant orthorhombic distortion of the complex. The theoretical calculations by Chandler *et al.*[12] are much less convincing in showing this difference. The diffuse 4p functions attain appreciable values but also have quite high uncertainties. However based on the results of the flexible multipole model it is reasonable to conclude that the 4p mixing is significant and that the theoretical calculations probably underestimate this component.

Conclusion

It has been shown that diffraction data measured on $Ni(ND_3)_4(NO_2)_2$ at very low temperatures cannot be explained by use of a simple valence-orbital model. This is consistent with results of a previous analysis of 9 K X–N diffraction data on $(ND_4)_2Cu(SO_4)_2\cdot 6D_2O$.[2,7] This study shows that detailed understanding of transition metal to ligand bonding requires a higher level of theory. To model the data adequately a very flexible electron-density model must be used. The chosen atom-centred multipole model describes the total electron-density distribution well, but it cannot express individual pseudo-atom properties. Owing to the very low temperature of the experiment a good deconvolution of the thermal motion has been achieved. The resulting static model density derived from the diffraction data has sufficient accuracy to allow topological analysis of the electron density. The topological analysis gives a detailed quantitative account of the metal–ligand interactions in the complex. The fact that precise topological information can be obtained even for transition-metal complexes opens up new possibilities for quantitative understanding of transition metal to ligand bonding. If topological information can be obtained on a number of complexes, trends and characteristics of the topology of various bonding types may be discovered.

Acknowledgements

B. B. I. gratefully acknowledges support for this work from the Danish Natural Science Research Council and the Carlsberg Foundation. The latter is thanked for the low-temperature diffractometer in Århus. The US Department of Energy is thanked for granting beamtime at the Intense Pulsed Neutron Source, Argonne National Laboratory. Work at Argonne is supported by the US Department of Energy, BES-Materials Science, under contract No. W-31-109-ENG-38. B. N. F. and P. A. R. acknowledge support from the Australian Research Council and Department of Industry.

References

1 B. N. Figgis and P. A. Reynolds, *Int. Rev. Phys. Chem.*, 1986, **5**, 265; P. Coppens, *Annu. Rev. Phys. Chem.*, 1992, **43**, 663.
2 B. N. Figgis, B. B. Iversen, F. K. Larsen and P. A. Reynolds, *Acta Crystallogr., Sect. B*, 1993, **49**, 794.
3 B. N. Figgis, L. Khor, E. S. Kucharski and P. A. Reynolds, *Acta Crystallogr., Sect. B*, 1992, **48**, 144.
4 See, for instance, F. K. Larsen, *Acta Crystallogr., Sect. B*, 1995, **51**, 468.
5 R. F. Stewart, *Acta Crystallogr., Sect. A*, 1976, **32**, 565; N. K. Hansen and P. Coppens, *Acta Crystallogr., Sect. A*, 1978, **34**, 909.
6 B. B. Iversen, F. K. Larsen, B. N. Figgis, P. A. Reynolds and A. J. Schultz, *Acta Crystallogr., Sect. B*, 1996, **52**, 923.
7 G. S. Chandler, B. N. Figgis, P. A. Reynolds and S. K. Wolff, *Chem. Phys. Lett.*, 1994, **225**, 421.
8 C. K. Johnson, ORTEP, Report ORNL-5138, Oak Ridge National Laboratory, Oak Ridge, TN, 1976.
9 (*a*) M. A. Porai-Koshits and L. M. Dikareva, *Sov. Phys.-Crystallogr.* (*Engl. Transl.*), 1960, **4**, 611; (*b*) B. N. Figgis, P. A. Reynolds, A. H. White, G. A. Williams and S. J. Wright, *J. Chem. Soc., Dalton Trans.*, 1981, 997; (*c*) B. N. Figgis, P. A. Reynolds and S. J. Wright, *J. Am. Chem. Soc.*, 1983, **105**, 434.
10 B. N. Figgis, P. A. Reynolds and G. A. Williams, *Aust. J. Chem.*, 1981, **34**, 993.
11 B. N. Figgis, P. A. Reynolds and R. Mason, *J. Am. Chem. Soc.*, 1983, **105**, 440.
12 G. S. Chandler, R. J. Deeth, B. N. Figgis and P. A. Reynolds, *J. Chem. Soc., Dalton Trans.*, 1990, 1417.
13 R. F. W. Bader, *Atoms in Molecules. A Quantum Theory*, Cambridge University Press, 1991.
14 (*a*) R. F. Stewart, in *The application of charge density research to chemistry and drug design*, eds. G. A. Jeffrey and J. F. Pinielle, *NATO ASI ser., Ser. B*, 1991, 250; (*b*) B. B. Iversen, F. K. Larsen, M. Souhassou and M. Takata, *Acta Crystallogr., Sect. B*, 1995, **51**, 580; (*c*) C. Flensburg, S. Larsen and R. F. Stewart, *J. Phys. Chem.*, 1995, **99**, 10 130; (*d*) R. Destro, R. Bianchi, C. Gatti and F. Merati, *Chem. Phys. Lett.*, 1991, **186**, 47; (*e*) R. Destro and F. Merati, *Z. Naturforsch., Teil A*, 1993, **48**, 99; (*f*) G. K. H. Madsen, B. B. Iversen, F. K. Larsen, M. Kapon, G. Reisner and F. Herbstein, unpublished work; (*g*) R. Destro and F. Merati, *Acta Crystallogr., Sect. B*, 1995, **51**, 559.
15 T. Koritzansky, S. Howard, P. R. Mallison, Z. Su, T. Richter and N. K. Hansen, XD, a computer program package for multipole refinement and analysis of charge densities from diffraction data, Institute for Crystallography, Berlin, 1995.
16 N. K. Hansen and P. Coppens, *Acta Crystallogr., Sect. A*, 1978, **34**, 909.
17 P. Becker and P. Coppens, *Acta Crystallogr., Sect. A*, 1974, **30**, 129.
18 E. Clementi and C. Roetti, *At. Data Nucl. Data Tables*, 1974, **14**, 177.
19 R. F. Stewart, E. R. Davidson and K. T. Simpson, *J. Chem. Phys.*, 1965, **42**, 3175.
20 P. Coppens, T. N. Guru Row, P. Leung, E. D. Stevens, P. J. Becker and Y. W. Yang, *Acta Crystallogr., Sect. A*, 1979, **35**, 63.
21 H. F. Schaefer, J. R. Thomas, Y. Yamaguchi, B. J. DeLeeuw and G. Vacek, *Modern Electronic Structure Theory*, ed. D. R. Yarkony, World Scientific, Singapore, 1995, p. 1.
22 M. W. Schmidt, K. K. Baldridge, J. A. Boatz, J. H. Jensen, S. Koseki, M. S. Gordon, K. A. Nguyen, T. L. Windus and S. T. Elbert, *QOPH Bull.*, 1990, **10**, 52.
23 (*a*) T. Kikkawa, S. Ohba, T. Saito, S. Kamata and S. Iwata, *Acta Crystallogr., Sect. B*, 1987, **43**, 83; (*b*) D. W. J. Cruickshank and M. J. Eisenstein, *J. Comput. Chem.*, 1987, **8**, 1, 6.
24 M. Okuda, S. Ohba, Y. Saito, T. Ito and I. Shibuya, *Acta Crystallogr., Sect. B*, 1990, **46**, 343.
25 S. Ohba, K. Toriumi, S. Sato and Y. Saito, *Acta Crystallogr., Sect. B*, 1978, **34**, 3535.
26 R. Bianchi, C. Gatti, V. Adovasio and M. Nardelli, *Acta Crystallogr., Sect. B*, 1996, **52**, 471.
27 R. Dovesi, V. R. Sauders and C. Roetti, CRYSTAL 92 User Documentation, University of Torino, 1992.

28 W. T. Klooster, S. Swaminathan, R. Nanni and B. M. Craven, *Acta Crystallogr., Sect. B*, 1992, **42**, 217.
29 B. Rees and A. Mitschler, *J. Am. Chem. Soc.*, 1976, **98**, 7918.
30 J. P. Collman, L. S. Hegedus, J. R. Norton and R. G. Finke, *Principles and applications of organotransition metal chemistry*, University Science Books, Mill Valley, CA, 1987.
31 R. F. W. Bader and H. Essen, *J. Chem. Phys.*, 1984, **93**, 2946; R. F. W. Bader, P. J. MacDougall and C. D. H. Lau, *J. Am. Chem. Soc.*, 1984, **106**, 1594.
32 B. N. Figgis, P. A. Reynolds and G. A. Williams, *J. Chem. Soc., Dalton Trans.*, 1980, 2339.
33 B. N. Figgis, E. S. Kucharski and P. A. Reynolds, *Acta Crystallogr., Sect. B*, 1989, **45**, 232.
34 B. N. Figgis, P. A. Reynolds and A. H. White, *J. Chem. Soc., Dalton Trans.*, 1987, 1737.

Received 21*st March* 1997; *Paper* 7/01978E